Adaptive-Neighborhood Speckle Removal in Multitemporal SAR Images

Mihai Ciuc[1,2], Philippe Bolon[1], Emmanuel Trouvé[1],

Vasile Buzuloiu[2], and Jean–Paul Rudant[3]

[1] Laboratoire d'Automatique et Micro-Informatique Industrielle,

Centre des Sciences Appliquées à la Production,

Ecole Supérieure d'Ingénieurs d'Annecy – Université de Savoie

41 avenue de la Plaine, BP 806 – 74016 Annecy Cedex, France

Tel : + 33 4 50 09 65 41, Fax : + 33 4 50 09 65 59

[2] Laboratorul de Analiza şi Prelucrarea Imaginilor,

Catedra de Electronică Aplicată şi Ingineria Informaţiei,

Universitatea "Politehnica" Bucureşti,

Bucharest, Romania

[3] Laboratoire de Géomatériaux

Institut Francilien des Géosciences

Université de Marne–la–Vallée

Marne–la–Vallée, France

{*ciuc*|*bolon*|*trouve*}*@esia.univ-savoie.fr,*

buzuloiu@alpha.imag.pub.ro,

rudant@univ-mlv.fr

Abstract: In this paper, we present a new method for multitemporal SAR image filtering using 3D adaptive neighborhoods. The method takes both spatial and temporal information into account to derive the speckle-free value of a pixel. For each pixel individually, a 3D adaptive neighborhood is determined to contain only pixels belonging to the same distribution as the current pixel. Then, statistics computed inside the established neighborhood are used to derive the filter output. It is shown that the method provides good results by drastically reducing speckle over homogeneous areas while retaining edges and thin structures. The performances of the proposed method are compared in terms of subjective and objective measures with those given by several classical speckle filtering methods.

Keywords: Synthetic aperture radar, Speckle, Image filtering, Adaptive neighborhoods.

1. Introduction

SAR image processing has become a rapidly developing field in the last decade, thanks to the large amount of data available from earth satellites such as JERS, ERS, Radarsat, etc. One of the major drawbacks of SAR images is that they are highly corrupted by speckle noise, which severely impedes automatic scene segmentation and interpretation. Thus, before attempting to process SAR images, a noise reduction step is necessary for most of the applications. According to Goodman [1], speckle is modeled as a multiplicative, i.e., signal–dependent, random process that corrupts the signal. Thus, filters dealing with speckle removal must be specifically designed to cope with the particularities of such a noise type. The most widely used filters are spatial filters, that take

into account spatial neighbors of a pixel to derive its output value [2, 3, 4, 5]. More recently, availability of multiple images of the same area acquired at regular time intervals (35 days for ERS satellites) broadened the application field of SAR images, by making possible investigation of temporal changes that may occur from an acquisition to another. Applications are attractive: studying the evolution of coastlines, deforestations, and agricultural areas [6, 7, 8]. Also, another SAR image filtering technique, temporal filtering, has become possible [9, 10]. The new filtered value of a pixel is computed with respect to its temporal neighborhood, i.e., using pixels at the same spatial location in different images. The main advantage is that spatial resolution is preserved.

In this paper we propose a new filter for multitemporal SAR images. The filter takes both temporal and spatial information into account, by determining, for each pixel, a 3D neighborhood that contains only pixels belonging to the same distribution as the current pixel. The proposed filter represents a very good trade–off between the spatial–only and temporal–only filters, by strongly reducing noise while preserving thin structures. The remainder of the paper is organized as follows: In Section **2.**, the multiplicative noise model is presented. Section **3.** presents a review of existing filtering methods. Section **4.** presents, in detail, the 3D adaptive–neighborhood filtering method. In Section **5.**, results obtained by the proposed filter are presented and compared to those provided by other filters. Section **6.** is dedicated to conclusions.

2. Speckle modeling

Let g denote the speckle image, f the ideal, speckle–free image, and let u be the multiplicative noise that is modeling speckle. The SAR image degradation model [1] is:

$$g = fu \tag{1}$$

with u being a signal–independent random variable whose probability density function (PDF) depends upon the image type. If g is a single–look intensity SAR image, the PDF of u is exponential:

$$p_u(x) = \begin{cases} \exp(-x) & \text{if } x \geq 0 \\ 0 & \text{otherwise} \end{cases} . \tag{2}$$

If g is a single–look amplitude image, then u can be modeled as a Rayleigh random variable:

$$p_u(x) = \begin{cases} 2x\exp(-x^2) & \text{if } x \geq 0 \\ 0 & \text{otherwise} \end{cases} . \tag{3}$$

Both intensity and amplitude images are very noisy (the signal–to–noise ratio of an intensity image is 0 dB!). Thus, a preprocessing step of SAR images is commonly applied to reduce the noise power at the expense of a spatial resolution degradation. The most frequently used preprocessing consists in incoherently averaging L different images obtained from the same image by dividing its Doppler frequency spectrum into L bands, thus yielding an *L–look* SAR image. The greater L, the better the achieved noise power reduction, but the poorer the resulting spatial resolution. The statistics of u in a multi–look SAR image are the following: for an L–look intensity image, u is Gamma distributed with parameter L:

$$p_u(x) = \begin{cases} \frac{L^L x^{L-1}}{\Gamma(L)}\exp(-Lx) & \text{if } x \geq 0 \\ 0 & \text{otherwise} \end{cases} , \tag{4}$$

with $\Gamma(L)$ being the Gamma function: $\Gamma(L) = \int_0^\infty t^{L-1}\exp(-t)dt$. For an L–look amplitude image (computed as the square root of an L–look intensity image for the sake of the mathematical model simplicity) the noise is distributed according to:

$$p_u(x) = \begin{cases} \frac{2L^L x^{2L-1}}{\Gamma(L)}\exp(-Lx^2) & \text{if } x \geq 0 \\ 0 & \text{otherwise} \end{cases} . \tag{5}$$

The noise standard deviation σ_u of an L–look intensity SAR image is $\sqrt{L}$ times smaller than in the original 1–look image. A more complex formula is derived as well to assess the noise standard

deviation reduction in an amplitude image. It should also be noted that, for all types of SAR images, the speckle PDF is non–symmetrical with respect to the mean value. This observation will be further addressed in Section **4.** .

The signal–dependent nature of speckle can be explained as follows: over homogeneous areas, i.e., areas locally characterized by $f \approx \overline{f}$, with$\overline{f}$ being the local mean, variations are due only to speckle. Over such areas, image values g are only realizations of speckle: $g_{hom} \approx \overline{f}\ u$. The speckle PDF over a homogeneous area $p_{g_{hom}}(x)$ can be expressed as:

$$p_{g_{hom}}(x) = \frac{1}{\overline{f}} p_u\left(\frac{x}{\overline{f}}\right), \tag{6}$$

with $p_u(x)$ given by one of the Equations (2)–(5). It follows that the speckle mean and standard deviation over featureless areas are given by:

$$\overline{g}_{hom} = \overline{f}\overline{u}, \tag{7}$$

$$\sigma_{g_{hom}} = \overline{f}\sigma_u. \tag{8}$$

According to Equation (8), the speckle standard deviation over uniform areas $\sigma_{g_{hom}}$ is proportional to the mean value $\overline{f}$ of the signal being corrupted. In other words, the noise power depends upon the intensity of the corrupted area: this makes bright regions in the image appear noisier than the dark ones.

3. Speckle filtering

It is obvious that standard filters designed for additive noise removal are not suitable for speckle filtering. Therefore, filters that take the multiplicative nature of speckle into account have been devised. In this section, an overview of the well–known speckle filtering methods is provided. In the first part, spatial filters aiming at speckle reduction using only spatial information, are presented. Then, the multichannel filtering techniques, that make use of the diversity of multiple SAR images of the same scene to filter out speckle are briefly reviewed.

A. Spatial filters

The best–known family of filters is the local–statistics filter family, the starting point of which is the Lee filter [2]. The idea is to compute the filter output $\hat{f}$ as to minimize the mean–squared error to the ideal noise–free pixel value f. The final result for the filtered value of a pixel is a linear combination of the current corrupted value and the statistical mean, the weights depending upon the signal and noise variances:

$$\hat{f} = \overline{f} + \frac{\sigma_f^2}{\sigma_g^2}(g - \overline{g}). \tag{9}$$

Since the statistical measures of the corrupted image (mean $\overline{g}$ and variance σ_g^2) are unknown, they are spatially estimated within a square neighborhood of the current pixel. Statistics of the ideal image are then deduced according to the assumed noise model. Even though computed with an exact formula for the additive noise case, the weights of the Lee filter are deduced only approximately in the multiplicative noise hypothesis, based on a linearization of the image degradation model. The final formula for the Lee filter is given in Equation (10):

$$\hat{f} = \frac{\overline{g}}{\overline{u}} + \frac{\overline{u}\left(\sigma_g^2\overline{u}^2 - \overline{g}^2\sigma_u^2\right)}{\sigma_g^2\overline{u}^4 + \overline{g}^2\sigma_u^4}(g - \overline{g}). \tag{10}$$

According to Equation (9), the behavior of the Lee filter can be described as follows: if the processing window overlaps an uniform image area, where variations are due only to noise, i.e., $\sigma_f^2 \approx 0$, the filter output will practically be the local mean. Thus, noise is strongly reduced over homogeneous areas. Conversely, if there is an edge within the neighborhood of the processed pixel, i.e., $\sigma_g^2 \approx \sigma_f^2$, the mean will be penalized and the filter output will practically be the noise–corrupted value of the current pixel. Thus, edges do not get blurred, even though noise still remains unfiltered in the vicinity of edges. Based upon the Lee filter model, many filtering schemes have been developed. Kuan et al. [4] derived the exact formula to compute the weights that appear in the Lee filter for

multiplicative noise as well:

$$\hat{f} = \frac{\overline{g}}{\overline{u}} + \frac{\sigma_g^2 \overline{u}^2 - \overline{g}^2 \sigma_u^2}{\sigma_g^2 \overline{u}^2 \left(\overline{u}^2 + \sigma_u^2\right)} (g - \overline{g}). \tag{11}$$

Another modification of the Lee filter weights was reported by Lopès et al. [11]. Frost et al. filter [5] is another local–statistics–based filter derived by using an approach slightly different from Lee's. Frost's filter is a spatially adaptive Wiener filter, the weights of which are computed to minimize the mean–squared error between the filtered and ideal values, in the hypothesis of multiplicative noise.

In Lee's sigma filter [3] only those pixels in the processing window whose values are within a threshold distance from the value of the current pixel participate in the filter output. The threshold is set at twice the local speckle standard deviation. The output of the Kuan et al. filter [12] is the maximum a posteriori estimator of the speckle–free value of the processed pixel, given the observation set formed by all pixels within a rectangular neighborhood. Arsenault and Levesque [13] proposed the homomorphic filtering for images corrupted by multiplicative noise. The idea is to transform the nature of noise from multiplicative to additive by means of applying a logarithmic transform to the image. The transformed image is then filtered using a filter devised for additive noise and back–transformed to the original space by the inverse logarithmic operator.

All of the above discussed filters are based on the use of a fixed–size processing window. Approaches to speckle filtering using local statistics computed within a variable–sized window have also been reported. Lee proposed a refined version of his filter [14] that performs noise reduction near sharp edges as well. In the enhanced version of the filter, the presence of an edge within the operating window is tested by comparing the standard deviation of signal σ_g with a given threshold T that may vary spatially according to the assumed noise model. If no edges are found, i.e., $\sigma_g < T$, all pixels within the window are used to compute the local statistics. If, on the contrary, an edge is detected, i.e., $\sigma_g \geq T$, the edge location is sought by computing the gradient along the four main

directions. Only pixels within the half–window that is limited by the edge and that contains the current pixel are used to compute the local statistics. Thus, noise is reduced near edges as well, since it can be considered that the data within the determined sub–window is uniform.

Wu and Maître [15] extended the idea of the refined Lee filter by computing the local statistics within as large a window as possible, instead of using a fixed–size window. Initially chosen as a square 3×3 window, the neighborhood size is successively increased as long as the overlapped image region remains uniform. If an edge is encountered, its position is determined. Only the sub–window containing the currently processed pixel and separated by the edge is further checked for expansion in the direction opposite to the edge. The isolated brilliant point model is also included. If a pixel is labeled as isolated brilliant point, i.e., the standard deviation computed within the 5×5 neighborhood is significantly lower than that computed within the 3×3 initial window, then only the 3×3 window statistics are used to determine the filter output. By using this approach, a better speckle reduction is expected, over homogeneous areas as well as near the edges, with no loss in detail preservation. Another adaptive–window based speckle reduction technique has been proposed by Park et al. [16].

Among the approaches — other than local–statistics based — to speckle filtering in SAR images, we should also mention Crimmins' geometrical filter [17] and the morphological filter developed by Safa and Flouzat [18].

All of the filtering techniques described above have been devised to deal with one single SAR image at a time. By their design, they are bound to degrade the spatial resolution of the image while filtering out speckle.

B. Multichannel filters

Improvements in SAR acquisition systems have made the acquisition of multipolarization and multifrequency SAR images possible. Moreover, spaceborne acquired multitemporal SAR data,

i.e., multiple coregistered images of the same area taken at constant time intervals, have become available. The diversity of images of the same scene allows the development of filters that aim at speckle removal using the additional information provided by the third dimension, regardless of its nature (polari-metric, frequential, or temporal).

Lin and Allebach [19] have developed the vector extension of Lee's local–statistics filter in the context of multifrequency SAR image processing. All available multifrequency SAR images of the same scene are treated as a vector image and a relation equivalent to that given in Equation (9) is derived for the multidimensional case to compute the filter output.

Lee et al. [9] have developed a filter that acts only on the third dimension for multipolarization and multifrequecy SAR images. Pixels at the same spatial locations in the different images are combined to yield the filtered value of a given pixel. Pixel weights are computed with respect to an optimality criterion. The filter output is a single image, the other filtered images being obtained by radiometric correction. The same idea was further investigated by Bruniquel and Lopès [10], in the context of multitemporal images. They derived the optimal weights using a more sophisticated SAR image model than that of Lee.

The advantage of such filters that act uniquely on the third dimension is that they do not reduce the spatial resolution. Meanwhile, due to the small number of images that are generally available, the speckle reduction achieved is not very important.

The filter proposed in this paper combines both spatial and temporal approaches to reduce speckle in multitemporal SAR images. Details of the proposed filter are provided in the following Section.

4. 3D adaptive–neighborhood filtering of SAR images

Most of neighborhood operators used in image processing are based on a fixed, generally square–shaped processing window. One drawback of such operators is that they are not sensitive to image characteristics that extend beyond the used neighborhood. Moreover, stationarity is not guaranteed even in small neighborhoods, such as 3×3. In order to better exploit the image information, the idea has come to use adaptive neighborhoods instead of fixed ones. Regardless of the application, the idea is to determine for *every* pixel of the image, called "seed" when processed, a variable–sized, variable–shaped neighborhood which contains only pixels whose value is close to that of the seed, i.e., pixels belonging to the same object as the seed. Then, only pixels within the established neighborhood are used to derive the new value of the seed. The adaptive neighborhood (AN) paradigm has been used in various applications, such as feature enhancement of mammograms [20], noise filtering in gray–level [21, 22, 23, 24] and color [25] images, and histogram equalization of gray–level [26] and color images [27]. Extension of the AN paradigm to the particular case of speckle filtering in multitemporal SAR images is detailed in the following Subsections.

A. Steps of the 3D adaptive neighborhood determination

In our approach to speckle filtering in multitemporal SAR images [28], we consider a sequence of N coregistered images of the same scene as a 3D volume, with two spatial and one temporal coordinates. For *every* pixel of the volume a 3D adaptive neighborhood has to be determined.

The proposed method is based on the statistical model of a homogeneous region, as given by Equation (6). This model is simpler and does not represent 2D textured regions. However, the adaptive neighborhood of a given pixel is a three–dimensional structure that contains both spatial and temporal neighbors of the seed. Thus, macro–textured areas can be represented by this model as well, provided thet they have temporal stability.

When a pixel is being processed, we want to aggregate in its AN only pixels that belong to the same homogeneous area, i.e., pixels the values of which differ one from another only because of speckle. Thus, speckle statistics must be taken into account in the AN determination procedure. As a measure of the membership of the value of a neighboring pixel p in the distribution of the currently processed pixel s, Lee [3] proposed to test the membership of $g(p)$ in the interval $[g(s) - 2\sigma_n,\ g(s) + 2\sigma_n]$, with σ_n being the noise standard deviation. We use the same basic idea, with some modifications based on the following observations:

- The speckle standard deviation $\sigma_{g_{hom}}$ is not a priori known, since it varies spatially. Still, it can be locally estimated as a function of the local mean $\overline{g}_{hom}$, as given in Equation (8).
- Since the current pixel value $g(s)$ is affected by noise, a more robust measure of the membership of a neighbor's value $g(p)$ in the distribution of $g(s)$ is obtained by checking the membership of $g(p)$ in the interval $[\overline{g}_{hom} - 2\sigma_{g_{hom}},\ \overline{g}_{hom} + 2\sigma_{g_{hom}}]$.
- As stated before, the speckle distribution over homogeneous areas is non–symmetrical with respect to the distribution mean. Thus, choosing a confidence interval which is symmetrical with respect to the mean is not appropriate, since this would induce a bias in the final result. To overcome this effect, the whole confidence interval is to be shifted by a quantity θ.

According to the observations above, the steps of the AN determination for a given seed pixel s are the following:

1. Coarsely estimate the local average $\overline{g}_{hom}$ as the median value g_{med} computed in a small 2D neighborhood (3×3 or 5×5) of the seed s.
2. Define a first confidence interval $[T_1, T_2]$ with

$$T_1 \quad = \quad g_{med} - \frac{\sigma_u g_{med}}{\overline{u}} + \theta, \tag{12}$$

$$T_2 \quad = \quad g_{med} + \frac{\sigma_u g_{med}}{\overline{u}} + \theta, \tag{13}$$

with θ computed as:

$$\theta = \epsilon \; g_{med}. \tag{14}$$

In Equation (14), ϵ is a proportionality factor whose computation is discussed in detail in Appendix A.

3. Compute an intermediate AN by means of a classical region growing algorithm: for every direct neighbor p of the seed in a $3 \times 3 \times 3$ neighborhood, the membership of its value $g(p)$ in the confidence interval is checked. If

$$g(p) \in [T_1, T_2],$$

the pixel p is retained in the neighborhood. Then, all 3D neighbors of the newly-included pixels are inspected in the same way, etc. The region growing process stops when either no other neighboring pixel meets the inclusion criterion, or the neighborhood size reaches a predefined limit N_{max}. The second stop condition is useful in order to avoid overloading the computational requirements of the algorithm. All pixels that were tested during this step but were not retained in the AN (referred to as "background pixels" in the sequel) are stored in a separate list.

4. Compute the mean $\overline{g}_{reg}$ of pixels already included in the AN.

5. Define a second confidence interval $[T_1', T_2']$ with

$$T_1' \quad = \quad \overline{g}_{reg} - 2\frac{\sigma_u \overline{g}_{reg}}{\overline{u}} + \theta, \tag{15}$$

$$T_2' \quad = \quad \overline{g}_{reg} + 2\frac{\sigma_u \overline{g}_{reg}}{\overline{u}} + \theta, \tag{16}$$

with parameter θ being computed at this stage as:

$$\theta = \epsilon' \; \overline{g}_{reg}. \tag{17}$$

6. Reinspect *only* the background pixels from the list they were stored in and retain them in the AN provided that their value $g(p) \in [T_1', T_2']$.

B. Justification of the AN determination steps

In this Subsection, the steps of the AN determination and the choice of the used parameters are discussed.

In the first step, the median g_{med} in a small 2D neighborhood is computed as an estimator of the region mean. The median of a pixel population is a not very precise estimator of the population mean. Still, using the median as mean estimator ensures that the estimation is not affected by outliers, i.e., pixels belonging to the same distribution but characterized by a strong deviation from the distribution mean. Based on the median value, the local standard deviation is computed as $\sigma_{g_{hom}} = g_{med}\,\sigma_u/\overline{u}$, as given by Equations (7) and (8). The value of the interval shifting parameter θ must be deduced with respect to the image type (intensity or amplitude), the number of looks L and the interval width $T_2 - T_1$. As shown in Appendix A, for the particular case of a confidence interval characterized by a width which is proportional to the distribution mean, the shifting parameter θ is also proportional to the distribution mean, which explains the value of θ in Equation (14).

Thus, a first, more selective confidence interval $[T_1,\ T_2]$ with thresholds T_1 and T_2 given by Equations (12) and (13) is defined and the AN grown with respect to it. Roughly speaking, a pixel is aggregated in the AN during the first step if its value is affected by an instance of speckle within a standard deviation from its mean. The advantage of using a first step region growing with a more selective inclusion criterion is twofold. Firstly, it reduces the probability that the AN grows over region boundaries. Secondly, it allows inclusion in the AN of an important sample of speckled pixels. The latter will be used in the second step to estimate the local mean more accurately.

All pixels checked for inclusion during the first step but not retained in the AN are marked as background pixels and stored in a separate list. Obviously, many of them should be taken into

account when computing the speckle–free seed value because they belong to the same distribution as the seed. But as they are affected by a stronger instance of noise, it made them unfit for retention in the AN at this stage of the algorithm. The appropriateness of their membership in the AN will be checked during the second step.

After the first step, the mean $\overline{g}_{reg}$ of pixels already aggregated within the AN is computed to stand for a more robust estimator of the local speckle mean $\overline{g}_{hom}$. The $\overline{g}_{reg}$ value is further used to estimate more precisely the local speckle standard deviation as $\sigma_{g_{reg}} = \overline{g}_{reg}\ \sigma_u/\overline{u}$ and the new interval shifting parameter θ as given by Equation (17). A more relaxed confidence interval $[T_1',\ T_2']$ is then defined by Equations (15) and (16). Parameter ϵ' is the proportionality factor between the distribution mean and the shifting parameter θ that corresponds to the new confidence interval width. Its computation is also discussed in Appendix A.

In the second step, only background pixels are reinspected for inclusion in the region with respect to the newly–defined confidence interval $[T_1',\ T_2']$. The reason for reinspecting only pixels that were previously checked is that, in most cases, most of them are located inside the region's convex hull. Hence, the risk of growing the region over a boundary is drastically reduced.

Figure 1 presents a typical histogram of pixels inspected during the determination of the adaptive neighborhood.

All pixels that were aggregated in the AN after the two region growing steps will participate in the computation of the filtered value of the seed, as detailed in the next Subsection.

C. Deriving the filtered seed value using adaptive neighborhood statistics

After determining the seed's AN, the mean $\overline{g}_{reg}$ and standard deviation σ_{reg} of pixels in the AN are computed. The new seed value is then derived according to Kuan's formula given in Equation (11), but using the AN statistics $\overline{g}_{reg}$ and σ_{reg} instead of the mean $\overline{g}$ and standard deviation σ_g computed within a fixed neighborhood. It should be mentioned that the correction term in Equation (11),

i.e., the one proportional with the quantity $g - \overline{g}$, is generally small. This could be expected, since the region ordinarily contains only pixels belonging to a single distribution, which, in addition, is truncated. It follows that the region mean $\overline{g}_{reg}$ by itself stands for a good estimator of the speckle–free seed value, even though Kuan's formula provides more robustness to the final speckle–free seed estimator.

5. Results and discussion

In this section, results obtained with the 3D adaptive neighborhood filter (hereafter 3D–ANF) are presented and compared to those given by other filtering algorithms. Among the spatial filters, we have chosen for comparison the refined Lee filter (RLF) [14] and the maximum homogeneous region filter (MHRF) [15], since these filters exhibit similar complexities. We have also chosen the Kuan filter [4], as being a reference filter in SAR imagery. From the temporal filter family, we have chosen the texture–compensation multitemporal filter (TCMF) proposed by Bruniquel and Lopès [10], since it seems to be the filter which has the best performances in its class. Since it can be argued that it is unfair to compare a filter that takes both spatial and temporal informations into account with filters based on spatial–only or temporal–only information, we have also used combinations of temporal and spatial filters: TCMF–Kuan, TCMF–RLF and TCMF–MHRF.

We tested all of the above filters on a sequence of PRI (PRecision Image) SAR images of the Saint–Laurent du Maroni area in the French Guyana provided by ERS–1 and ERS–2 satellites. The sequence includes six 2300×2400 pixel, 16–bit, 3–look, amplitude images.

A. Selection of the parameters of the filters

For the Kuan and refined Lee filters, we used a 7×7 processing window, since it turned out to be the most suitable choice for the trade–off between speckle reduction and structure preservation. In the case of MHRF, the choice of the three thresholds used to decide if the data in the processing window

is uniform, or if there is a brilliant point within the processing window, raised some problems. The authors did not explain, in detail, the way of computing the thresholds, and restricted themselves to indicating the values they used for a specific application. After thorough testing, we chose the following threshold values: $T_1 = 21$, $T_2 = 10$, $T_3 = 60$. In the case of 3D–ANF, we limited the growth of the region in the first step to $N_{max} = 100$, since tests conducted on many image sets had shown that there is no real improvement in the final results for higher values of N_{max}. For the temporal–spatial filtering combination, the speckle reduction achieved by temporal filtering was taken into accound in the spatial filtering by accordingly modifying the multiplicative noise standard deviation σ_u.

B. Subjective assessment of the performances of the discussed filters

In the case of Kuan's filter the speckle reduction is associated with a slight edge blurring effect. Moreover, some artifacts due to speckle still remain in the filtered image. The RLF is more satisfactory than Kuan's filter, as it achieves better noise attenuation in the vicinity of edges too. Moreover, edges are sharper than in the case of Kuan's filter.

The non–adaptive nature of thresholds, which does not suit the multiplicative noise model, reduces the performances of MHRF. However, the MHRF also attenuates speckle and preserves edges. A general remark for all of the spatial filters is that the resulting filtered image has a "patchy" look, which is a known effect of purely spatial filtering. This effect is the most pronounced for the MHRF, whereas the RLF is less affected.

The purely temporal filtering stands no comparison with spatial filtering in what concerns speckle reduction, which is normal, due to the small number of pixels that participate in the derivation of the output value. However, some noise attenuation can be noticed after TCMF. The most interesting part of TCMF is that there is practically no loss in resolution. Fine features, which are hardly visible in the original images, and which are lost after spatial filtering, become noticeable

after TCMF. This makes TCMF attractive if the final goal is visual inspection of SAR images.

As for the combination of purely temporal and purely spatial filterings, no substantial improvement in comparison with the spatial–only approach can be noticed. This is mostly due to the poor speckle reduction achieved by temporal filtering. Moreover, the improvements obtained by purely temporal filters are completely lost after a spatial filtering step.

The 3D–ANF provides the best overall results: speckle is drastically reduced over homogeneous areas, whereas thin structures are preserved. Thanks to the large number of pixels of the same distribution that are averaged to yield the filter output, the speckle reduction is more important than in the case of the other spatial filters. Of course, the feature preservation provided by 3D–ANF is less important than that achieved by TCMF, due to the fact that spatial averaging occurs during 3D–ANF as well. However, the fact that the AN of a pixel is allowed to grow along the "temporal" axis contributes to a smaller degradation of spatial resolution, and, thus, to a less pronounced "patchy" effect.

Another aspect to be discussed in the case of 3D–ANF is the preservation of temporal information. Figure 2 presents the results obtained after applying the 3D–ANF on an image portion that contains a rice field characterized by strong temporal variations. As previously mentioned, temporal changes that occur between two acquisions are of a high relevance for SAR image users. Thus, they are to be preserved. In this regard too, the 3D–ANF provides good results. A temporal change is treated in the same way as a spatial edge, i.e., the AN of a pixel located near a "temporal" edge will grow space–wise, whereas temporal neighbors on the other side of the edge will most likely not be included in the AN.

Figures 3 and 4 present the original and filtered versions of a 512×512 sub–image from one of the six images of the sequence.

C. Comparison between filters with respect to objective criteria

For the objective comparison of the filtering performances, we use the criteria introduced by Lee et al. [29] to assess the noise reduction, the edge preservation, and the mean value retention achieved by the different filtering methods. The following subsections discuss the objective comparison between the presented filters in detail.

1. Speckle reduction

The speckle strength is related to the ratio:

$$\beta = \frac{\sigma_{g_{hom}}}{\overline{g}_{hom}} \tag{18}$$

which is supposed to be constant over a homogeneous region of the image, regardless of its average value. The smaller β, the better the speckle reduction. Another criterion alternative to β is the equivalent number of looks (ENL) computed as:

$$\text{ENL} = \frac{1}{\beta^2} \tag{19}$$

for an intensity SAR image, and as

$$\text{ENL} = \left(\frac{0.522}{\beta}\right)^2 \tag{20}$$

in the case of an amplitude SAR image.

The ENL of a filtered image represents the number of bands of a single–look image that should be incoherently averaged to achieve the same speckle reduction as the respective filtering method. In order to assess the speckle reduction, four featureless areas of about the same size, 200×200 pixels, characterized by different average values were cropped from the image set. The results are presented in Table 1.

As indicated by parameter β, the 3D–ANF provides the better speckle reduction over homogeneous areas, followed by the RLF. The MHRF and Kuan filters provide similar performances,

whereas the TCMF has the poorest noise reduction, as stated before. No significant improvement can be noticed by performing a temporal filtering prior to filtering spatially with any of the spatial filters.

2. Edge preservation

As a measure of the edge preservation, Lee proposed to compute the gradient G across a contour, and the sum S of variances computed within two narrow strips located on both sides of the contour. The gradient G stands for a measure of the edge sharpness, whereas the sum of variances S allows the assessment of the method's capability to filter speckle near edges.

In order to compute the parameters above, two areas of 216×216 and 128×128 pixels containing an edge were clipped off. The narrow strips along the contour were drawn manually. Figure 5 shows the two areas and the selected strips. Then, for each contour, the G and S measures were computed as:

$$G = |\mu_{\text{strip 1}} - \mu_{\text{strip 2}}|, \tag{21}$$

$$S = \sigma^2_{\text{strip 1}} + \sigma^2_{\text{strip 2}} \tag{22}$$

where $\mu_{\text{strip i}}$ and $\sigma_{\text{strip i}}$ represent the mean and standard deviation computed by using pixels contained in strip i, $i \in \{1, 2\}$. The numerical results are presented in Table 2.

It can be noticed that 3D–ANF provides a better contour preservation than other filters. Moreover, 3D–ANF achieves the best speckle filtering in the vicinity of edges, as indicated by the parameter S. RLF provides good noise reduction near edges as well, which was expected, since this was the purpose it was designed for. The Kuan filter and MHRF provide similar performances, followed by the TCMF. Here again, we can notice that the temporal–spatial filtering combination provides no significant improvement in comparison with the purely spatial filtering.

3. Mean preservation

Another factor that characterizes a filtering method is the preservation of the mean value. Table 3 presents the mean values over the homogeneous areas used for evaluation of speckle reduction.

From the point of view of the induced bias in the average reflectivity, it appears that the 3D–ANF performances are the poorest. This can be explained by the fact that the interval width used in the region growing procedure is proportional to the estimated local average. Thus, in some cases, a region grown from a dark noisy pixel located within an area characterized by a higher local average cannot grow properly, due to the underestimation of the latter. A solution would be to increase the confidence interval limits, but this would lead to poorer overall results. Moreover, the induced bias is within acceptable limits (about 3%) and it does not affect the visual appearance of the filtered image. The same trend can be remarked in the case of MHRF, whereas all of the other filters do not introduce any bias.

4. Computational time

The computational time is another factor that must be taken into account when comparing different filtering methods. Table 4 summarizes the times taken by all of the filtering methods for filtering the sequence of six, 2300×2400 pixel, 16 bit/pixel images on a Sun Ultra 10 workstation with a clock rate of 440 MHz, 500 MB of memory and 1 MB of cache memory. All filtering methods were implemented using the standard C programming language.

As expected, the fastest methods are Kuan and RLF, followed by MHRF. The TCMF is slower, whereas the 3D–ANF takes the longest time. The two latter methods are penalized by the fact that they treat all the images at a time. This implies allocation of very large memory blocks, which slows down the algorithm, due to frequent hard–disk operations (swapping). Running the programs on more powerful machines would improve the time performances of TCMF and 3D–ANF more

than in the case of the other three methods. Another possibility of reducing the computational time would be code optimization, or parallel execution, but this is beyond the scope of the present paper.

6. Conclusion

In this paper, a new method for filtering multitemporal SAR images has been presented. For each seed pixel in the SAR image sequence viewed as a volume, a 3D adaptive neighborhood is derived to contain only pixels that are similar to the considered pixel. Then, statistics computed using only pixels in the adaptive neighborhood are used to derive the seed filtered value. It is shown that the proposed filtering method provides better results than other classical speckle filtering algorithms, from a subjective point of view, as well as objectively, as given by several quantitative criteria. The speckle reduction achieved by the proposed method, along with its spatial and temporal detail preservation capabilities make it a powerful tool for multitemporal SAR image preprocessing.

Appendix A: Computation of the bias reduction shifting parameter

In this section, the computation of the shifting parameter θ used to reduce bias with respect to the image type, the number of looks and the interval width is presented. The speckle PDF over featureless areas $p_{g_{hom}}(x)$ given in Equation (6), regardless of the image type or of the number of looks, is not symmetrical with respect to its mean. Thus, if we estimate the speckle mean using only pixels whose values lie within an interval centered around its mean as:

$$\hat{\overline{g}}_{hom} = A \int_{\overline{g}_{hom}-T}^{\overline{g}_{hom}+T} x \; p_{g_{hom}}(x) \; dx, \tag{23}$$

the result $\hat{\overline{g}}_{hom}$ will always be an underestimation of the real mean value $\overline{g}_{hom}$. This is due to the fact that the area computed over the left interval $\overline{g}_{hom} - T$ is always larger than that over the right interval $\overline{g}_{hom} + T$. In Equation (23), A represents a normalization constant. Thus, both interval

limits must be increased by a quantity θ to compensate for this effect. The situation is illustrated in Figure 6.

Parameter θ must be computed so that the estimated mean over the interval $[\overline{g}_{hom} - T + \theta,\ \overline{g}_{hom} + T + \theta]$ equals the real mean value $\overline{g}_{hom}$:

$$B \int_{\overline{g}_{hom}-T+\theta}^{\overline{g}_{hom}+T+\theta} x\ p_{g_{hom}}(x)\ dx\ = \overline{g}_{hom}, \tag{24}$$

with

$$B = \left(\int_{\overline{g}_{hom}-T+\theta}^{\overline{g}_{hom}+T+\theta} p_{g_{hom}}(x) dx \right)^{-1}. \tag{25}$$

In the case of intensity SAR images, Equation (24) leads to the following expression:

$$\left(\frac{\overline{g}_{hom} - T + \theta}{\overline{g}_{hom} + T + \theta} \right)^{L} = \exp\left(-\frac{2LT}{\overline{g}_{hom}} \right) \tag{26}$$

that finally yields the value of θ:

$$\theta = \frac{1 + \exp\left(-\frac{2T}{\overline{g}_{hom}}\right)}{1 - \exp\left(-\frac{2T}{\overline{g}_{hom}}\right)} T - \overline{g}_{hom}. \tag{27}$$

For the specific values of T used in the two AN determination steps, $T = \sigma_{g_{hom}}$, and $T = 2\sigma_{g_{hom}}$ respectively, we remark that the corresponding values of θ are proportional to the speckle mean $\overline{g}_{hom}$ since $\sigma_{g_{hom}} \propto \overline{g}_{hom}$ as indicated in Equation (8). This is the reason why the shifting term θ in Equations (12), (13), (15), and (16) has been set as proportional to the mean. The values of the constants ϵ, to be used in Equation (14), and ϵ', to be used in Equation (17) for an intensity SAR image are:

$$\epsilon = \frac{1 + \exp\left(-\frac{2}{\sqrt{L}}\right)}{1 - \exp\left(-\frac{2}{\sqrt{L}}\right)} \frac{1}{\sqrt{L}} - 1 \tag{28}$$

$$\epsilon' = \frac{1 + \exp\left(-\frac{4}{\sqrt{L}}\right)}{1 - \exp\left(-\frac{4}{\sqrt{L}}\right)} \frac{2}{\sqrt{L}} - 1 \tag{29}$$

$$\tag{30}$$

For a SAR amplitude image, Equation (24) has no analytical solution. The value of θ can be numerically approximated for specific values of the number of looks L and of threshold value T.

Note that ϵ and ϵ' are fixed for a given image. Thus, they must be determined at the beginning and need not be recomputed during the filtering procedure.

Acknowledgments

We thank the GdR–ISIS for supporting this work within the framework of the Programme National de Télédétection Spatiale (PNTS '98) project, and the European Space Agency (ESA) for providing the images.

References

1. J. W. Goodman. Some fundamental properties of speckle. *Journal of the Optical Society of America*, 66(11):1145–1149, 1976.

2. J. S. Lee. Digital image enhancement and noise filtering by use of local statistics. *IEEE Trans. Pattern Anal. Machine Intell.* , 2:165–168, March 1980.

3. J. S. Lee. Digital noise smoothing and the sigma filter. *Computer Graphics and Image Processing*, 24:255–269, 1983.

4. D. T. Kuan, A. A. Sawchuk, T. C. Strand, and P. Chavel. Adaptive noise smoothing filter for images with signal–dependent noise. *IEEE Trans. Pattern Anal. Machine Intell.* , 7:165–177, 1985.

5. V. S. Frost, J. Abbot Stiles, K. S. Shanmugan, and J. C. Holtzman. A model for radar images and its application to adaptive digital filtering of multiplicative noise. *IEEE Trans. Pattern Anal. Machine Intell.* , 4(2):157–165, March 1982.

6. E. J. M. Rignot and J. J. van Zyl. Change detection techniques for ERS–1 SAR data. *IEEE Trans. on Geoscience and Remote Sensing*, 31(4):896–906, July 1993.

7. S. Quegan, T. Le Toan, J. J. Yu, F. Ribbes, and N. Floury. Multitemporal ERS SAR analysis applied to forest mapping. *IEEE Trans. on Geoscience and Remote Sensing*, 38(2):741–753, March 2000.

8. H. Trébossen, J. P. Rudant, B. Fruneau, and N. Classeau. Contribution of SAR imagery for mapping coastal's areas: examples of sedimentationnal and erosionnal zones in French Guiana and Mauritania. In *Proc. of* 6^{th} *Intl. Conf. on Remote Sensing for Marine and Coastal Environments*, volume 2, pages 398–405, Charleston, South Carolina, USA, 2000. Veridian ERIM International, Ann Arbor.

9. J. S. Lee, M. R. Grunes, and S. A. Mango. Speckle reduction in multipolarization, multifrequency SAR imagery. *IEEE Trans. on Geoscience and Remote Sensing*, 29(4):535–544, July 1991.

10. J. Bruniquel and A. Lopès. Multi–variate optimal speckle reduction in SAR imagery. *International Journal on Remote Sensing*, 18(3):603–627, 1997.

11. A. Lopès, R. Touzi, and E. Nezry. Adaptive speckle filters and scene heterogeneity. *IEEE Trans. on Geoscience and Remote Sensing*, 28(6):992–1000, November 1990.

12. D. T. Kuan, A. A. Sawchuk, T. C. Strand, and P. Chavel. Adaptive restoration of images with speckle. *IEEE Trans. on Acoustics, Speech and Signal Processing*, 35(3):373–383, March 1987.

13. H. H. Arsenault and M. Levesque. Combined homomorphic and local–statistics processing for restoration of images degraded by signal–dependent noise. *Applied Optics*, 23:845–850, March 1984.

14. J. S. Lee. Refined filtering of image noise using local statistics. *Computer Graphics and Image Processing*, 15:380–389, 1981.

15. Y. Wu and H. Maître. Smoothing speckled synthetic aperture radar images by using maximum homogeneous region filters. *Optical Engineering*, 31(8):1785–1792, August 1992.

16. J. M. Park, W. J. Song, and W. A. Pearlman. Speckle filtering of SAR images based on adaptive windowing. *IEE Proceedings - Vision, Image and Signal Processing*, 146(4):191–197, 1999.

17. T. R. Crimmins. Geometric filter for speckle reduction. *Applied Optics*, 24(10):1438–1443, October 1985.

18. F. Safa and G. Flouzat. Speckle removal on radar imagery based on mathematical morphology. *Signal Processing*, 16:319–333, 1989.

19. Q. Lin and J. P. Allebach. Combating speckle in SAR images: vector filtering and sequential classification based on a multiplicative noise model. *IEEE Trans. on Geoscience and Remote Sensing*, 28(4):647–653, July 1990.

20. R. Gordon and R. M. Rangayyan. Feature enhancement of film mammograms using fixed and adaptive neighborhoods. *Applied Optics*, 23(4):560–564, April 1984.

21. R. B. Paranjape, R. M. Rangayyan, and W. M. Morrow. Adaptive neighborhood mean and median filtering. *Journal of Electronic Imaging*, 3:360–367, October 1994.

22. R. B. Paranjape, T. F. Rabie, and R. M. Rangayyan. Image restoration by adaptive neighborhood noise subtraction. *Applied Optics*, 33:1861–1869, May 1994.

23. R. M. Rangayyan and A. Das. Filtering multiplicative noise in images using adaptive region–based statistics. *Journal of Electronic Imaging*, 7:222–230, 1998.

24. R. M. Rangayyan, M. Ciuc, and F. Faghih. Adaptive–neighborhood filtering of images corrupted by signal–dependent noise. *Applied Optics*, 37(20):4477–4487, May 1998.

25. M. Ciuc, R. M. Rangayyan, T. Zaharia, and V. Buzuloiu. Filtering noise in color images using adaptive–neighborhood statistics. *Journal of Electronic Imaging*, 9(4):484–494, October 2000.

26. R. B. Paranjape, W. M. Morrow, and R. M. Rangayyan. Adaptive–neighborhood histogram equalization for image enhancement. *CVGIP:Graphical Models and Image Processing*, 54:259–267, 1992.

27. V. Buzuloiu, M. Ciuc, R. M. Rangayyan, and C. Vertan. Adaptive–neighborhood histogram equalization of color images. *Journal of Electronic Imaging*, 10(2):445–459, April 2001.

28. M. Ciuc, Ph. Bolon, E. Trouvé, and H. Trébossen. Multitemporal SAR image filtering using 3D adaptive neighborhoods. In S. Serpico, editor, *Image and Signal Processing for Remote Sensing VI*, volume 4170 of *Proc. SPIE*, pages 1–12. SPIE, 2000.

29. J. S. Lee, I. Jurkevich, P. Dewaele, P. Wambacq, and A. Oosterlink. Speckle filtering of synthetic aperture radar images: a review. *Remote Sensing Reviews*, 8:313–340, 1994.

FIGURE CAPTIONS

1. Histogram of pixels inspected during the determination of the adaptive neighborhood. Solid line: pixels selected during the first step of region growing. Dashed line: background pixels included during the second step. Dotted line: background pixels not included in the adaptive neighborhood.

2. Image parts used for assessing edge preservation. Left column: Original edge–containing parts of images. Right column: Strips manually drawn along edges.

3. Results of different speckle filtering algorithms: (a) original 512×512 pixel part of a 3–look amplitude image from a six–image multitemporal sequence; (b) image after Kuan filtering; (c) image after RLF; (d) image after MHRF.

4. Results of different filtering algorithms on the original image in Figure 3.a: (a) image after TCMF; (b) image after TCMF, followed by RLF; (c) image after TCMF, followed by MHRF; (d) image after 3D–ANF.

5. Preservation of temporal information. Left column: 512×512 pixel portions of three successive original images containing rice fields changing from one acquisition to the other. Right column: images filtered using 3D–ANF.

6. The speckle PDF over a homogeneous area of a 3–look intensity image of average intensity $\overline{g}_{hom} = 100$. The speckle standard deviation $\sigma_{g_{hom}} = \overline{g}_{hom}/\sqrt{L} \approx 58$. $\epsilon \approx 0.11$. The dashed line corresponds to the distribution mean value. In dashdotted lines, the limits of the centered interval $[\overline{g}_{hom} - \sigma_{g_{hom}},\ \overline{g}_{hom} + \sigma_{g_{hom}}]$. In dotted lines, the limits of the interval to be used in order to avoid biased estimation $[\overline{g}_{hom}(1+\epsilon) - \sigma_{g_{hom}}, \overline{g}_{hom}(1+\epsilon) + \sigma_{g_{hom}}]$.

Table 1. Values of parameter β for different featureless image areas

	Area 1 $\overline{g}_{hom} = 178$	Area 2 $\overline{g}_{hom} = 289$	Area 3 $\overline{g}_{hom} = 361$	Area 4 $\overline{g}_{hom} = 389$
Original	0.342	0.331	0.326	0.329
RLF	0.168	0.170	0.144	0.157
MHRF	0.197	0.204	0.189	0.193
Kuan	0.195	0.209	0.187	0.196
TCMF	0.255	0.249	0.238	0.250
TCMF–RLF	0.165	0.167	0.146	0.153
TCMF–MHRF	0.194	0.199	0.190	0.191
TCMF–Kuan	0.194	0.203	0.186	0.193
3D–ANF	0.148	0.155	0.119	0.134

Table 2. The G and S parameters used to assess edge preservation

	Edge 1		Edge 2	
	G_1	S_1	G_2	S_2
Original	148	206	220	165
RLF	138	118	210	99
MHRF	135	127	209	114
Kuan	129	131	200	119
TCMF	146	173	215	142
TCMF–RLF	142	118	212	96
TCMF–MHRF	138	127	210	113
TCMF–Kuan	131	130	201	119
3D–ANF	149	97	220	75

Table 3. The mean value over uniform areas

	Area 1	Area 2	Area 3	Area 4
Original	178	289	361	389
RLF	178	288	359	387
MHRF	175	282	350	377
Kuan	178	289	360	388
TCMF	178	288	359	388
TCMF–RLF	178	287	360	387
TCMF–MHRF	175	283	351	377
TCMF–Kuan	178	288	359	388
3D–ANF	175	276	351	376

Table 4. Computational time (in minutes) for the six–image, 2300 × 2400 pixel/image, 16 bit/pixel sequence

RLF	MHRF	Kuan	TCMF	3D–ANF
10'	33'	9'	65'	125'

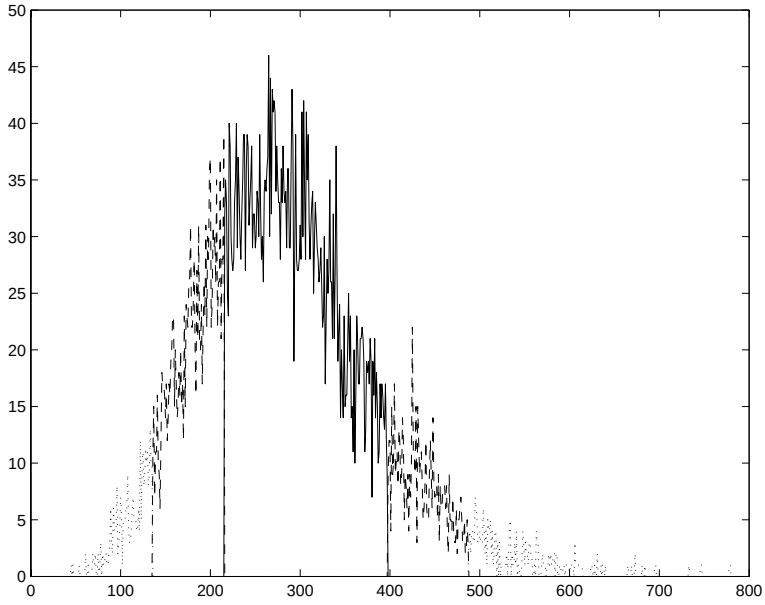

Fig. 1. Histogram of pixels inspected during the determination of the adaptive neighborhood. Solid line: pixels selected during the first step of region growing. Dashed line: background pixels included during the second step. Dotted line: background pixels not included in the adaptive neighborhood.

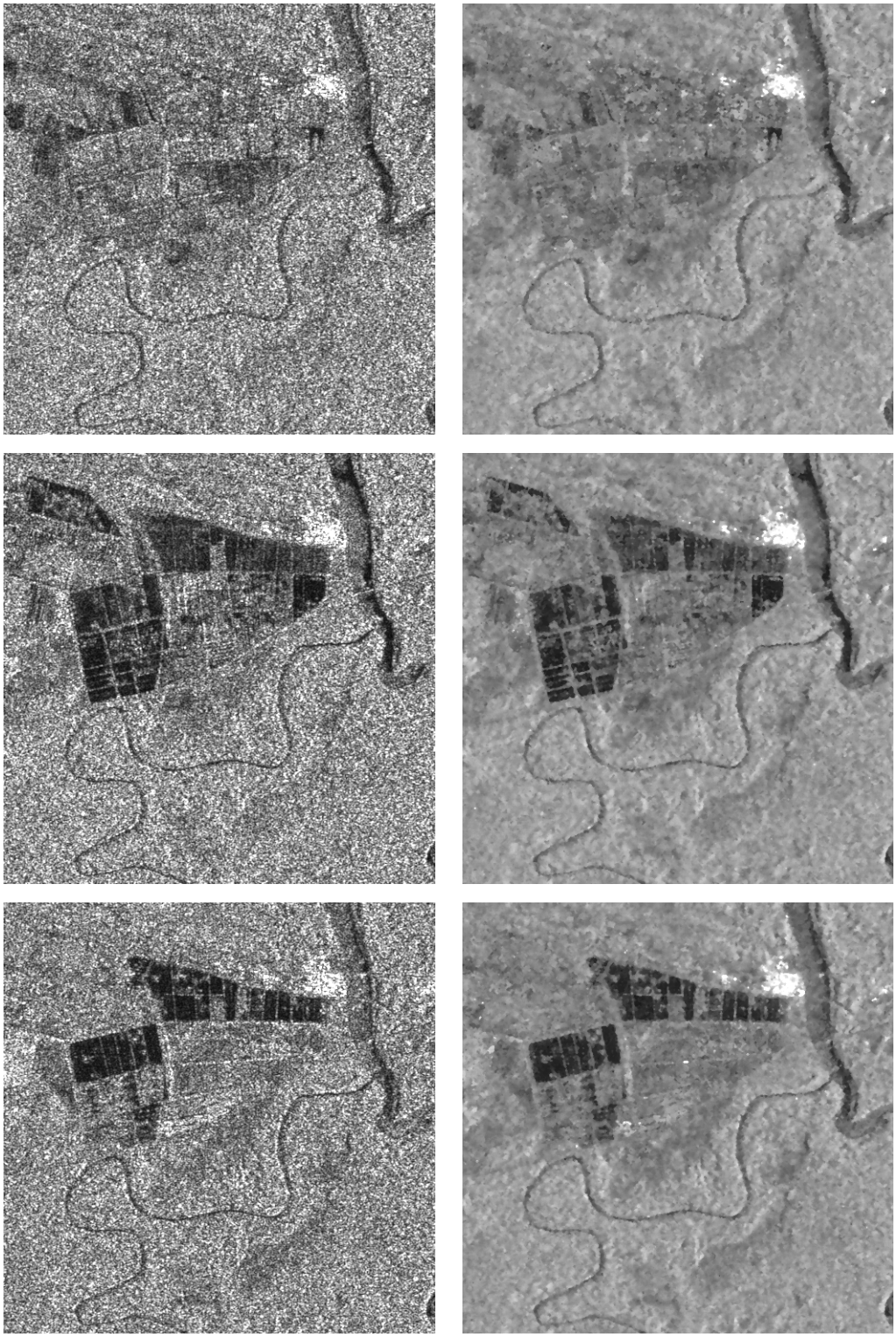

Fig. 2. Preservation of temporal information. Left column: 512×512 pixel portions of three successive original images containing rice fields changing from one acquisition to the other. Right column: images filtered using 3D–ANF.

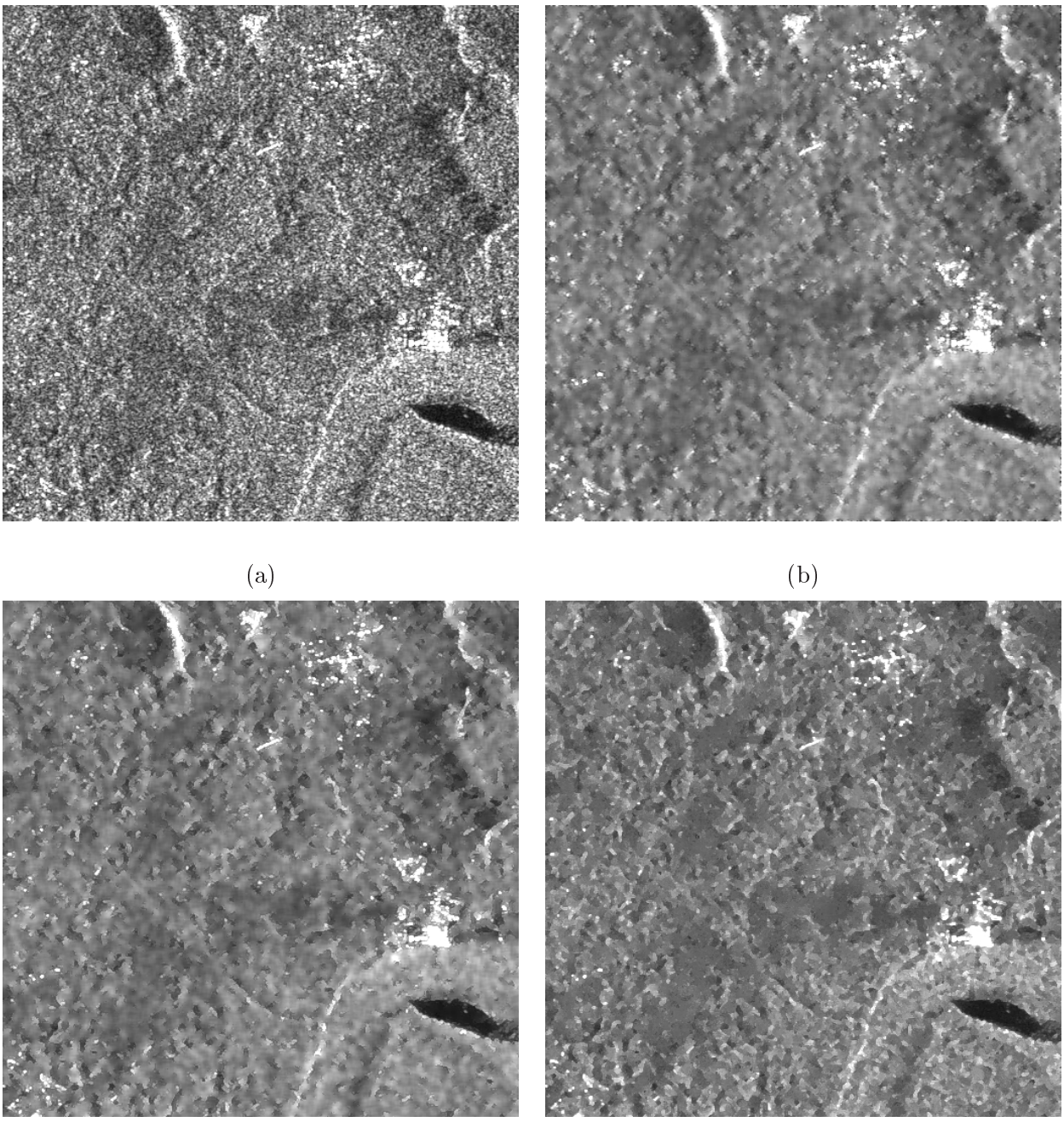

(a) (b)

(c) (d)

Fig. 3. Results of different speckle filtering algorithms: (a) original 512×512 pixel part of a 3–look amplitude image from a six–image multitemporal sequence; (b) image after Kuan filtering; (c) image after RLF; (d) image after MHRF.

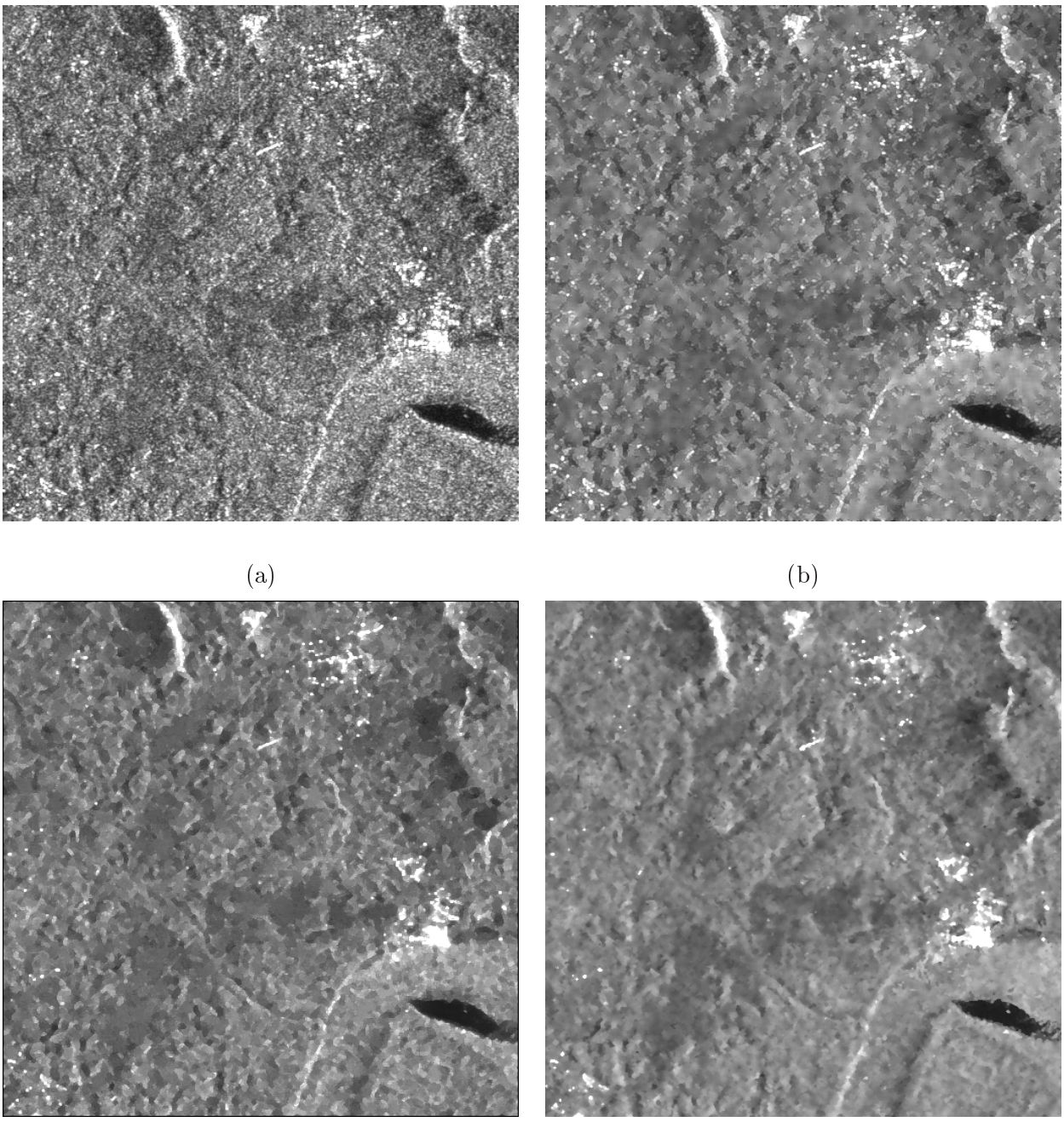

(a) (b)

(c) (d)

Fig. 4. Results of different filtering algorithms on the original image in Figure 3.a: (a) image after TCMF; (b) image after TCMF, followed by RLF; (c) image after TCMF, followed by MHRF; (d) image after 3D–ANF.

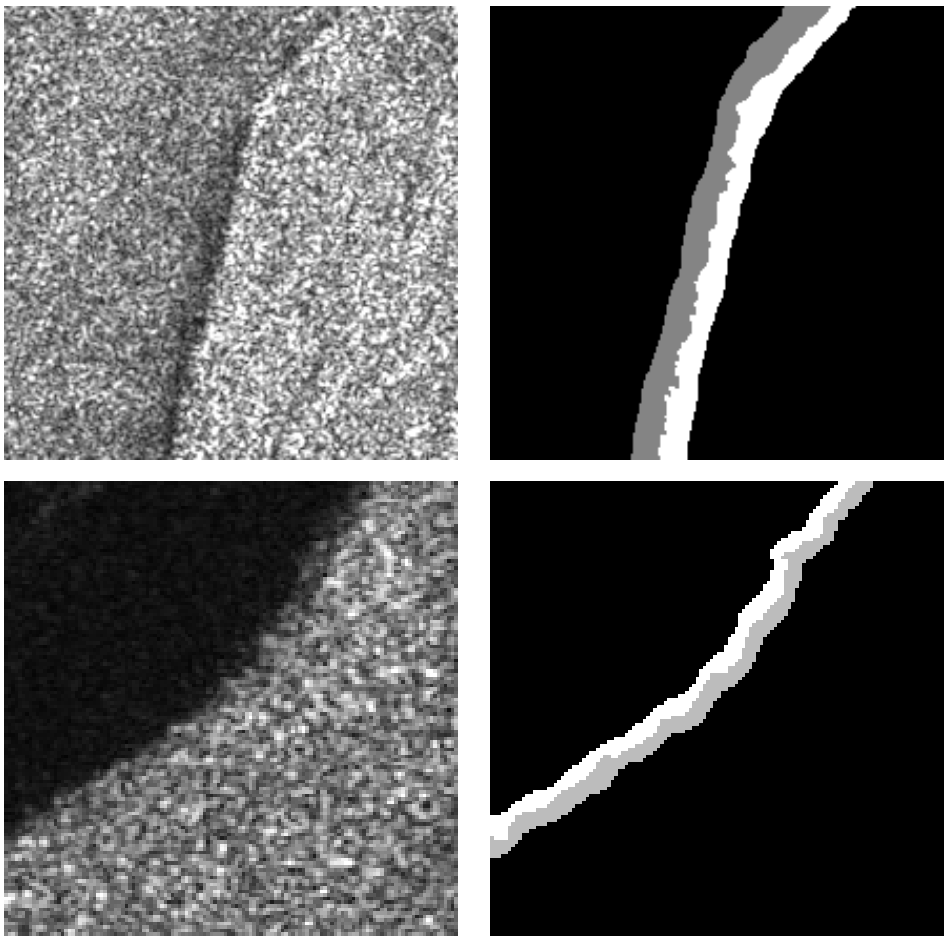

Fig. 5. Image parts used for assessing edge preservation. Left column: Original edge–containing parts of images. Right column: Strips manually drawn along edges.

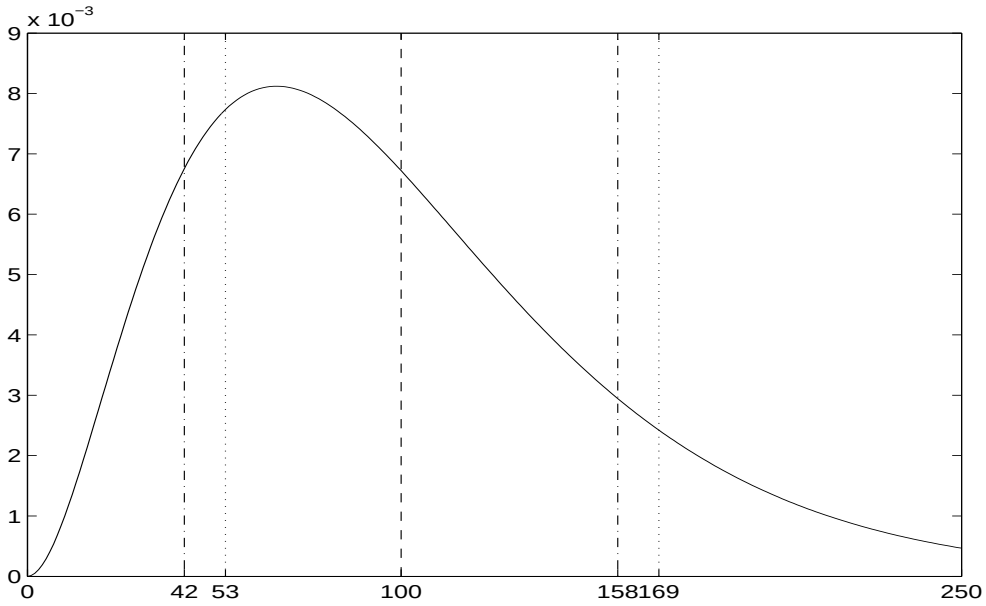

Fig. 6. The speckle PDF over a homogeneous area of a 3–look intensity image of average intensity $\overline{g}_{hom} = 100$. The speckle standard deviation $\sigma_{g_{hom}} = \overline{g}_{hom}/\sqrt{L} \approx 58$. $\epsilon \approx 0.11$. The dashed line corresponds to the distribution mean value. In dashdotted lines, the limits of the centered interval $[\overline{g}_{hom} - \sigma_{g_{hom}}, \overline{g}_{hom} + \sigma_{g_{hom}}]$. In dotted lines, the limits of the interval to be used in order to avoid biased estimation $[\overline{g}_{hom}(1+\epsilon) - \sigma_{g_{hom}}, \overline{g}_{hom}(1+\epsilon) + \sigma_{g_{hom}}]$.